Article

Insights on the interfacial processes involved in the mechanical and redox stability of BaCeZrYO3-#-CeGdO composite.

Cecilia Mortalò, Marta Boaro, Elena Rebollo, Valentina Zin,
Eleonora Aneggi, MONICA FABRIZIO, and Alessandro Trovarelli

Just Accepted

Insights on the interfacial processes involved in the

mechanical and redox stability of

$BaCe_{0.65}Zr_{0.2}0Y_{0.15}O_{3-\delta}$-$Ce_{0.85}Gd_{0.15}O_{2-\delta}$ composite.

Cecilia Mortalò[§], Marta Boaro[+]*, Elena Rebollo[§], Valentina Zin[§], Eleonora Aneggi[+],

Monica Fabrizio[§], Alessandro Trovarelli[+].

+ Dipartimento Politecnico di Ingegneria e Architettura, University of Udine, Via Cotonificio 108, 33100 Udine.

§ Consiglio Nazionale delle Ricerche (CNR), Istituto di Chimica della Materia Condensata e di Tecnologie per l'Energia (ICMATE), Corso Stati Uniti 4, 35127, Padova, Italy

KEYWORDS: dual phase ceramic composites, temperatures programmed analyses, redox behavior, proton conductors, ceria-based oxides.

1

ABSTRACT: Ceramic fuel cells and H_2 permeation membranes are key technologies to accelerate the transition from a carbon economy based on fossil fuels to a H_2 economy based on the use of renewable resources. The competitiveness of these technologies on market depends on the identification and optimization of stable and effective low-cost materials. Perovskite-fluorite ceria-based composites show suitable properties and studies on the mechanism that rules their mechanical, thermal and redox stability are crucial for further technological advances. This study focuses on the redox behavior of $BaCe_{0.65}Zr_{0.20}Y_{0.15}O_{3-\delta}$-$Ce_{0.85}Gd_{0.15}O_{2-\delta}$ (BCZY-GDC) dual phase ceramic. Temperature programmed reduction, thermogravimetry and temperature dependent X-ray diffraction and Raman analyses are used to understand the dynamics of the interaction between the ceramic oxide components. It is shown how the simultaneous occurrence of structural changes in BCZY and GDC reduction helps decreasing the mechanical stresses induced by temperature and by the reducing atmosphere. The interfacial processes between the single GDC and BCZY oxides contribute to limit reduction of GDC in the composite, which allows a complete reversibility of the redox process investigated in this study. Thus, it is suggested that redox behavior of this class of materials may be a descriptor of their mechanical and thermal stability.

2

1. INTRODUCTION

Nowadays, social, economic, and environmental issues related to the use of fossil fuels boost towards a rapid transition to a sustainable and cleaner energy system based on renewable resources. In this prospective, hydrogen as energy vector has been considered a fundamental key enabling technology.[1,2] A strategy for accelerating this transition could be the optimization and strengthening of hydrogen related-technologies that make use of fossil fuel as feedstock. Examples of this approach are the use of membranes for hydrogen purification in the conventional hydrocarbons reforming processes and the spreading of intermediate temperature solid oxide fuel cell (IT-SOFC) technology among the highly efficient electrochemical approaches to produce electric power.[3] The progress of protonic and mixed protonic-electronic conductors[4-15] as well as the development of new materials with multifunctional conduction properties is crucial for the advancement of both membranes and IT-SOFC technologies[16-21]. An approach to tune the conductivity of materials according to their area of application is the preparation of two-phase composites containing oxides with different types of conductivity. The combination of perovskite and fluorite phases based on cerium oxide is often explored to tune proton and oxygen ions conductivity of IT-SOFC electrolytes[16,17] and the mixed ion-electronic conductivity of hydrogen-selective ceramic membranes.[10,18] This may offer many advantages; for example by integrating two proton and oxygen conductive phases, it is possible to enhance materials conductivity and the power-out of ceramic fuel cells at lower temperature.[22]

Low temperature of operation potentially lowers the cost of these systems due to reduced stack and balance-of plants constraints, while it improves their reliability and stability to thermal cycles. In addition, fast transport of protons at low temperature favors kinetics and thermodynamics for higher-value chemicals production through processes such as hydrogenation/dehydrogenation.[9]

On the other hand, the use of protonic-electronic conductors for H_2 selective membranes as an alternative to Pd-based materials offers the advantage of a cost-effective separation process with improved chemical and mechanical robustness. Moreover, protonic-electronic membranes can operate at higher temperatures, which favors an easier integration with cascade industrial processes that require pressurized and hot hydrogen.[10,11]

In the context of this latter application, we have recently developed a mixed proton-electron conductor based on $BaCe_{0.65}Zr_{0.20}Y_{0.15}O_{3-\delta}$ (BCZY) and$Ce_{0.85}Gd_{0.15}O_2$ (GDC), which resulted to be one of the most effective membrane for H_2 separation at 750°C with good robustness towards CO_2 containing atmosphere[19,20] and acceptable tolerance to H_2S impurity.[21] The optimization of this material stems from previous studies on individual components. The use of neutron and high-resolution diffraction techniques and Raman spectroscopic studies have provided an understanding of the correlations among structure, composition and conductivity for both the cerate-zirconate[23-29] and gadolinium-doped cerium oxide.[30,31] These studies have contributed to rationalize the behavior of BCZY-GDC composite under operating conditions. The proton conduction and H_2 transport in BCZY occurs through the Grotthuss mechanism. This mechanism involves a specific reorientation of the hydroxides and the transfer of protons by hopping between adjacent oxygen ions.[32,33] It implies an ambipolar diffusion of protons and electrons and also of hydroxyl groups (in presence of oxygen vacancies and water). The reduction of Gadolinium-doped cerium oxide, which generally starts in the range of 500-600°C[34,35], promotes the enhancement of the electronic conductivity and concentration of oxygen vacancies in the dual phase material, thus boosting proton conductivity and hydrogen transport above 600°C. On the other hand, such a composite showed a potential mechanical fragility when exposed to hydrogen flow at high temperature. In fact, proton incorporation and reduction of Ce^{4+} to the larger Ce^{3+} cation cause expansion of BCZY and GDC lattice[36,37]

4

respectively, with consequent mechanical strains that could affect the performance and lifespans of devices based on this material.

Recently, we have demonstrated the importance of fundamental studies on the composite to ascertain its stability under operating conditions.[38] The study showed that under reducing and humidified environment BCZY and GDC behave synergistically with their expansion coefficients converging towards a common value, thus favoring the mechanical stability of BCZY-GDC based systems.

In this study we gained insights into the mechanism that contributes to mitigate the effect of lattice expansion of the two oxides in the composite. Thermogravimetry (TGA), temperature programmed reduction (TPR), X-ray diffraction (XRD) and Raman spectroscopy were used to investigate the BCZY-GDC synergistic behavior during a redox cycle. In spite of the fact that the functionality of the material strongly depends on reduction and oxidation behavior, to the best of our knowledge this is the first study that focuses on redox properties of the composite. We found that an interfacial process can explain the mechanical and redox stability of the composite under reducing conditions, suggesting that the redox behavior of perovskite-fluorite materials could be used as a good descriptor of their mechanical and thermal stability.

2. EXPERIMENTAL SECTION

Preparation of materials.

$BaCe_{0.65}Zr_{0.2}Y_{0.15}O_{3-\delta}$ (BCZY) powder was purchased from Marion Technologies (France) while $Ce_{0.85}Gd_{0.15}O_{2-\delta}$ (GDC) powder was prepared by solid state reaction.[19] In order to obtain the composite BCZY-GDC, the two powders were ball milled in proportion 46 wt% (BCZY) and 54wt% (GDC) following a previously reported procedure.[19] Milling was carried out on

5

powders suspended in ethanol for 1 h with zirconia balls (Pulverisette 6, Fritsch). Afterwards, the mixture was dried, grinded in a mortar and sieved in the range 45-150 meshes.

In order to study materials with properties similar to those encountered in membrane and electrolyte applications, the powders were pelletized and sintered under air at high temperature (1450°C) and then grinded and sieved through 45 and 150 meshes. Physico-chemical properties of powders are reported in a previous study.[19]

Characterization techniques

XRD analyses: XRD analyses were performed by using a Philips X'Pert diffractometer operating at 40 kV and 40 mA using nickel-filtered Cu K(alpha) radiation. Phase identification was done from the diffractograms recorded with a step size of 0.02° and a counting time of 40 s per angular abscissa in the range of 20–145 2θ degrees. Rietveld refinement of XRD pattern was performed by means of GSAS-EXPGUI program.[39,40]Diffractograms were also collected using a hot chamber (Anton Park) after reduction and oxidation ramps. The reducing gas was a mixture of 4.58% H_2 in N_2, while air flow was used for the oxidative ramp. Dry gases were fed through stainless steel lines from tanks. In both reducing and oxidizing ramp each sample was heated at 10°C/min from RT to 750°C and diffractograms were collected after 30' isotherm at the set point temperature (50°C, 200°C, 350°C, 550°C, 750°C). To avoid structural changes during XRD acquisition the counting time was shortened to 15s and the 2θ degrees range was set from 20 to 100. The experiments were conducted following this procedure: (i) reduction ramp from RT to 750°C, (ii) isothermal step at 750°C for 120', (iii) cooling to 50°C, (iv) purging in N_2 15', (iiv) oxidation at 500°C for 1h and then (v) oxidation ramp to 750°C.

Raman analyses: Raman spectra were collected with an Xplora Plus confocal Micro-Raman system (Horiba, Japan) on sample powders deposited on a thin glass used in

6

microscopy for optical observations. BCZY and GDC materials showed a different adsorption of Raman source; therefore, the conditions used for the comparison were optimized to obtain an acceptable response for both materials. The Raman spectra were collected in the range 50-1200 cm^{-1} using a 532nm Nd:YAG laser at the power of 7.1 mW with a grating filter of 2400 cm^{-1}. The accumulation time was 18-20s with two scans. The comparison of the results has been made among normalized spectra corrected for their baseline. The results were analyzed by fitting the Raman spectra with the proprietary software LabSpec6. The *in situ* experiments were carried out in a Linkam CR100 chamber by using 20-30 mg of samples. Before the redox cycle, all the specimens were pretreated in air at 600° C to clean the surface. This procedure also allowed powders to settle in the sample holder, ensuring a good reproducibility of the results. The redox cycle consisted of an oxidizing ramp (10°C/min) up to 740°C in air flow (30cc/min) as reference followed by a reducing ramp in 4.58%H$_2$ in N$_2$ flow (30cc/min) up to 800°C. Spectra were recorded every 20°C or 40°C with a stabilization time of 20 s. After reduction the samples were re-oxidized at 600°C **(Figure S1).** The final effect of redox cycle was checked at room temperature by recording spectra in at least four points of the sample.

Temperature programmed reduction (TPR) analyses: TPR experiments were carried out in a Micromeritics Autochem II 2920 analyser under a 4,58% H$_2$/N$_2$ flow passing through the sample (35 STP cc/min) with a ramp of 10 °C/min from room temperature up to 940°C. The samples were previously oxidized at 500°C for 1h to eliminate adsorbates such as carbonates and hydroxyl groups. The signal was left to equilibrate in the atmosphere of reaction for 30' before starting the heating ramp. The equilibrated signal at room temperature was used as reference for drawing a base line. H$_2$ consumption was quantified by a standard calibration procedure as already reported.[41] Two consecutive temperature programmed reductions were carried out on the composite alternating an oxidation step in air at 900°C for 1h.

7

Thermogravimetric analyses: Thermogravimetric analyses of as-prepared samples were carried out under a 4.58% H_2 in N_2 flow (100 cc/min) using a Q500 thermo balance (TA Instruments). The gas flow was transversal to the surface of the sample. The reduction occurred in isothermal conditions at 200°C, 350°C, 550°C, 750°C, 900°C.

3. RESULTS AND DISCUSSION

X-ray analysis

The structural changes of the single oxides and of BCZY-GDC composite during redox cycles were studied by *in-situ* X-ray diffractometry. X-ray diffractograms of the samples at room temperature are shown in **(Figure S2)**. The obtained profiles confirmed our previous results;[38] GDC crystallizes in a cubic phase (*Fm3m*) while BCZY shows an orthorhombic symmetry (*Imma*). BCZY diffractogram showed also small peaks at 34, 48, and 57 2θ degrees, which were attributed to the presence of a small impurity of Y_2O_3 in the material.[19] The XRD of the BCZY-GDC composite results from the overlap of the profiles of the single components.

During thermal treatment in reducing atmosphere we observed changes in the shape and in the positions of peaks of BCZY **(Figure 1a)**, while GDC peaks showed a gradual shift to lower 2θ angles as temperature increased without any change in their shape **(Figure 1b).**

8
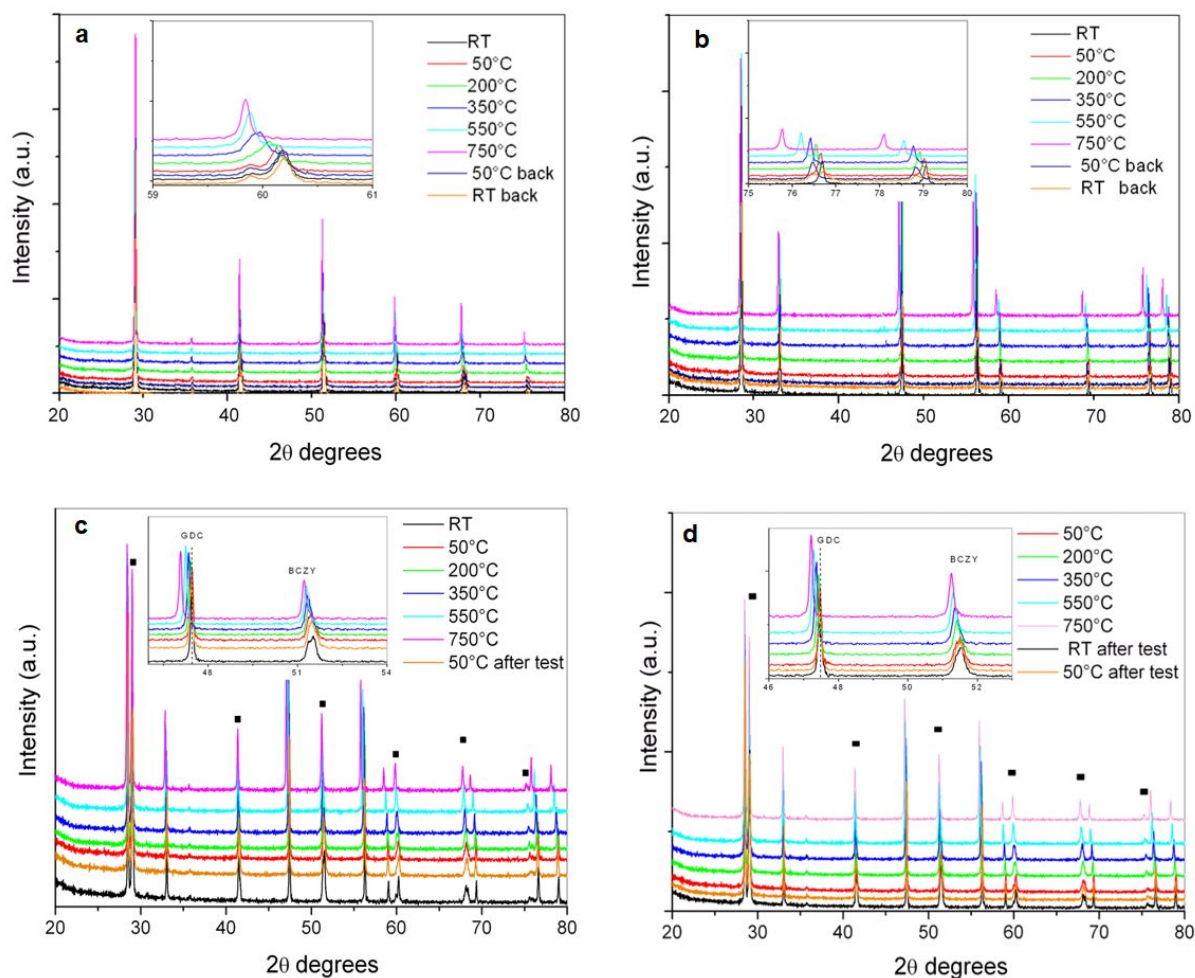
Figure 1. X-Ray diffractograms recorded in 4.58% H_2/N_2 flow with a heating ramp of 10°C/min for BCZY (a); GDC (b) and BCZY-GDC (c), and recorded in air for BCZY-GDC (d). The insert shows details to highlight changes during the heating ramp. In (c) and (d) peaks belonging to BCZY phase are indicated (■).

BCZY underwent a first phase transition from an orthorhombic (*Imma*) structure to a trigonal phase (*R-3c*) around 200°C and then a second transition to a cubic phase (*Pm-3m*) above 500°C **(Figure S3)**. These results well agree with previous observations collected at the synchrotron Petra III (DESY Synchrotron, Hamburg).[38] **(Table 1)** shows the results of Rietveld refinement of some representative diffractograms proving that the transitions were

reversible and independent on the treatment atmosphere (see also **Figure S4)**. BCZY peaks were also observed to shift to lower 2θ angles by increasing the temperature up to 550°C. Above this temperature the displacement was visible only for the peaks at high angles. This result correlated with the thermal expansion of the BCZY lattice during the heating ramp. After the redox cycle the volume of the cell returned back to the initial value.

GDC did not show modifications of the cubic symmetry during the thermal treatments in both oxidizing and reducing atmospheres, showing a shift of all peaks towards lower 2θ angles as the temperature increased (Figure 1b) and **(Figure S5)**. Below 550°C the shift was independent on the atmosphere of treatment and due to mechanical expansion related to the increase of temperature. Above 600°C we recorded a larger shift under reducing conditions since at this temperature the thermal expansion of GDC lattice occurs together with the reduction of Ce^{4+} to Ce^{3+}, which introduces cations of larger size into the structure of GDC. TPR and TGA analyses confirmed the reduction of the oxide above 600°C.

(Figure 1c and Figure **1d)** and (**Table 2**) summarize the XRD analyses for the BCZY-GDC composite during the thermal treatment, under reducing and oxidizing atmosphere, respectively. Under both conditions, thermal behavior reflected that of bare components: GDC as well as BCZY phase showed peak shift to lower 2θ angles up to 750°C, with a larger displacement for peaks of GDC exposed to reducing atmosphere at high temperature (above 600°C). However, at 750°C, the cell parameter of GDC lattice in the composite resulted slightly smaller than that of the single oxide (5.4793 Å *vs.* 5.4830 Å), probably because of a minor contribution of the reduction process to the thermal expansion. The cooling to room temperature restored the initial profile, leaving the two phases in the composite structurally unaltered.

10

Table 1. Rietveld refinement results of selected diffractograms for BCZY and for GDC collected during reduction and oxidation ramps[a].

Sample	Temp [°C]	Ramp	Phase	Cell parameters [Å]	Pseudo cubic Volume [Å³]
BCZY	50	H_2/N_2	orthorhombic	a=6.1550(2) b=6.1764(2) c=8.6781(2)	82.48(17)
	550	H_2/N_2	cubic	a=4.3657(7)	83.21(42)
	750	H_2/N_2	cubic	a=4.3847(1)	84.296(1)
	50	H_2/N_2	orthorhombic	a=6.1562(2) b=6.1786(2) c=8.6785(2)	82.53(17)
	50	air	orthorhombic	a=6.1566(2) b=6.1786(2) c=8.6785(2)	82.53(17)
	500	air	cubic	a=4.3742(1)	83.692(3)
	750	air	cubic	nd[b]	nd
	50	air	orthorhombic	a=6.1555(2) b=6.1768(2) c=8.6810(2)	82.51(57)
GDC	50	H_2/N_2	cubic	a=5.4165(2)	158.914(23)
	550	H_2/N_2	cubic	a=5.4510(81)	161.969(5)
	750	H_2/N_2	cubic	a=5.4830(1)	164.837(3)
	50	H_2/N_2	cubic	a=5.4284(1)	159.958(3)
	50	air	cubic	a=5.4160(1)	158.868(2)
	550	air	cubic	a=5.4510(1)	161.971(5)
	750	air	cubic	a=5.4639(1)	163.117(5)
	50	air	cubic	a=5.4252(1)	159.678(2)

[a] sequence of treatment: (i) ramp in H_2 (4.58%)/N_2 starting from 50°C to 750°C and then back to 50°C (ii) treatment in air at 500°C (iii) ramp in air from 50°C to 750°C and then back to 50°C; [b] we limited the oxidation ramp for BCZY up to 500°C, since previous studies did not show significant structural changes above this temperature.[38]

Summarizing, diffraction data indicates that BCZY underwent two phase transitions during the thermal treatment either in oxidizing or reducing atmosphere. These structural changes were reversible and took place together with thermal expansion that reached its maximum at 750°C. The thermal behavior of the single phase was the same of that observed for the phase in the composite. GDC, either as single phase or in the composite, did not change its structure during the thermal treatments, but a lattice expansion occurred whose entity depended on

11

treatment atmosphere. The maximum thermal expansion was obtained in reducing environment at 750°C, due to the additional effect of Ce^{4+} reduction. Under such operating conditions, thermal expansion of GDC in the composite was smaller, suggesting that the reduction of Ce^{4+} in GDC was hindered by the co-presence of BCZY.

A perusal of the results reported in Table 1 and 2 reveals that the final cell parameters of BCZY and GDC single oxides obtained after the ramps of reduction and oxidation were slightly larger than that measured at the beginning of thermal treatment, suggesting tiny structural and compositional changes underwent by the single components during redox cycles (see Figure S5 and related comment). Moreover, complete reversibility of the thermal behavior of BCZY-GDC was observed, which can be associated to the high stability of composite.[38]

Table 2. Rietveld refinement results of selected diffractograms for the BCZY-GDC composite collected during reduction and oxidation ramps[a].

Sample	Temp [°C]	Ramp	Phase	Cell parameters [Å]	Pseudo cubic Volume [Å³]
BCZY	50	H_2/N_2	orthorhombic	a=6.1404(3) b=6.1695(3) c=8.6774(5)	82.18 (20)
	550	H_2/N_2	cubic	a=4.3702(7)	83.468 (4)
	750	H_2/N_2	cubic	a=4.3817(1)	84.126 (4)
	50	H_2/N_2	orthorhombic	a=6.1377(2) b=6.1675(2) c=8.6813(2)	82.16 (21)
GDC	50	H_2/N_2	cubic	a=5.4179(1)	159.036(6)
	550	H_2/N_2	cubic	a=5.4524(1)	162.077(6)
	750	H_2/N_2	cubic	a=5.4793(1)	164.500(6)
	50	H_2/N_2	cubic	a=5.4229(1)	159.476(6)
BCZY	50	air	orthorhombic	a=6.1404(3) b=6.1707(3) c=8.6761(4)	82.19(19)
	550	air	cubic	a=4.3699(5)	83.448(3)
	750	air	cubic	a=4.3802(7)	84.04(40)
	50	air	orthorhombic	a=6.1398(3) b=6.1686(3) c=8.6786(5)	82.17(19)
GDC	50	air	cubic	a=5.4181 (1)	159.050(6)
	550	air	cubic	a=5.4501 (1)	161.891(3)
	750	air	cubic	a=5.4652 (1)	163.237(6)
	50	air	cubic	a=5.4198 (1)	159.204(5)

[a] sequence of treatment:(i) ramp in H_2 (4.58%)/N_2 starting from 50°C to 750°C and then back to 50°C (ii) treatment in air at 500°C (iii) ramp in air from 50°C to 750°C and then back to 50°C

Raman analysis

To gain insights into the role of interfacial properties of the two oxides and into the nature of their interaction in the composite we performed *in-situ* Raman temperature programmed redox experiments. Raman analysis is in fact a powerful technique to investigate the local short distance structural properties and the defects arrangement of ceria based materials[42,43] and to follow structural changes of protonic conductor perovskite oxides[27,29,44]

   (Figure 2) shows the Raman spectra of the as prepared BCZY, GDC and BCZY-GDC (see SI for details in the analysis, **(Figure S6, S7, S8)** and **(Table S1)**).
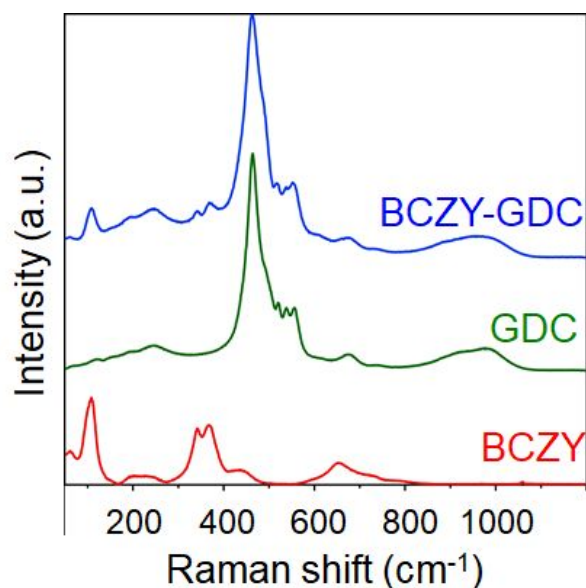
13

Figure 2. Comparison of normalized Raman spectra of BCZY, GDC and BCZY-GDC.

BCZY profile is characterized by peaks at about 61 cm^{-1}, 108 cm^{-1}, 218 cm^{-1}, 341 cm^{-1}, 367 cm^{-1}, 434 cm^{-1} and 654 cm^{-1}. The tiny peak at 1056 cm^{-1} (see Figure S8) is attributed to OH groups embodied into the lattice.[44] The peaks are typical of a rhombohedral structure as reported by Tu et al.[27] The peaks at 108 cm^{-1}, 341 cm^{-1} and 367 cm^{-1} could be attributed to the three E_g mode of R3c-phase.[27,28,45] The different position of peaks compared to the reference is due to the specific composition analyzed in this study. The bands in the range of 340 - 370 cm^{-1}, which were associated with the X-O (X=Ce, Zr, Y) stretching modes, are in fact sensitive to the cerium content in the BCZY system. The weak shoulder at 434 cm^{-1} is attributed to a symmetrical radial breathing mode of the six oxygen ions around Ce^{4+} in the perovskite structure. The band in the range of 550-900 cm^{-1} could be related to vibration stretching modes of Zr-O bonds.[46] The increase of the intensity/frequency of this band has been related to the transition from rhombohedral to cubic phase.[27] On the other hand, the

14

presence of this band in cubic perovskites could be indicative of the presence of oxygen vacancies into the lattice.[47]

Raman results contrast with XRD findings which showed the formation of stable *Imma* orthorhombic structure at room temperature. The structure of cerates - zirconates at room temperature depends on their composition and degree of hydration.[48]   Many studies reported diagrams that rationalize the structural evolution of BCZ and/or BCZY according to the amount of cerium.[27,29] Generally, for molar yttrium content of 0.1-0.2 it is identified a threshold value of cerium molar content above which the orthorhombic or monoclinic structure would be stabilized. This value is in the range of 0.6-0.7 depending on the characterization techniques used. Neutron and Synchrotron X-ray diffraction studies reported a monoclinic structure for a composition identical to that under investigation.[29] On the other hand, the rhombohedral structure detected here agrees with the diagram designed through Raman studies[27] for $Ba(Zr_{0.8-x}Ce_xY_{0.20})O_{2.9}$ compositions. The sample studied in this work contains an amount of cerium which falls within the range of critical values for the assessment of BCZY phase transition from rhombohedral to orthorhombic. The discrepancy of results between Raman and XRD analyses can be justified based on a higher sensitivity of Raman spectroscopy to the detection of structural transitions compared to X-ray diffractometry. On the other hand, our results are also compatible with the Raman potentiality of short-to-medium structural analysis to identify microdomains of different composition and higher symmetry, which may be present in the oxide.

GDC spectrum shows small and overlapped peaks at 116 cm^{-1}, 167 cm^{-1}, 193 cm^{-1} and 246 cm^{-1}, an asymmetric intense band at 463 cm^{-1}, with a shoulder at 486 cm^{-1}, a series of peaks in the range of 520-610 cm^{-1}, a less intense peak at 674 cm^{-1} and a broad band around 807-1088 cm^{-1}. According to the literature, the most intense peak is due to the F_{2g} symmetric vibration mode of Ce—O bond in an eightfold configuration, which is typical of CeO_2 fluorite

15

compounds. Peaks at 248 cm^{-1} and those at 522, 538, and 557 cm^{-1} are instead related to the introduction of Gd into the fluorite structure with the creations of vacancies within the Gd coordination sphere.[49,50] Recently DFT calculation and experimental studies demonstrated that the band at about 560 cm^{-1} resulted from the stretching vibration of O atom between M^{3+} and Ce^{4+} ions near oxygen vacancies.[51] Therefore it was correlated to the existence of intrinsic vacancies due to non-stoichiometric conditions of the oxides (substitution of Ce^{4+} with Ce^{3+} cations).[52] The peak above 600 cm^{-1} was attributed to the formation of ReO$_8$-type complex due to the substitution of Ce by Gd, with no oxygen vacancies, but participating to the formation of Frenkel oxygen defects.[53] The band above 800 cm^{-1} was related to the presence of peroxides and superoxides.[54]

In the spectrum of the BCZY-GDC composite, we observed the typical peaks of both BCZY and GDC components; however, the peaks related to the GDC were more intense. This is consistent with the composition of the material (that contains 54 wt.% of GDC) and with a different adsorption of the two oxides (Figure S7 and S8). The spectrum shows some difference from that calculated by the combination of the spectra of the single components as observable in **(Figure S9)**; these differences are mainly found in the relative intensity of the bands of the two components and in the shape of bands linked to the presence of defects and vacancies. The intensity ratio between relevant bands are summarized in **(Table S2)**. In more detail: (1) The ratio between intensity (I) area of band at ∼ 560 cm^{-1} and ∼ 463 cm^{-1} (R=I560/I463), which is often referred as a measure of the oxygen vacancies and of the reducibility of rare earth doped ceria oxides,[51,55] resulted smaller for the composite (R=0.1) compared to that for the pure GDC (R=0.23), thus indicating a lower reduction of the former. (2) The tiny differences in the range of 460-580 cm^{-1} existing between the pure GDC and the composite could be due to an alteration of the electronic environment of vacancies due to the presence of BCZY/GDC interfaces. (3) The attenuation of the peaks belonging to BCZY in

16

the composite (at 108 cm^{-1}, 339-370 cm^{-1}, and at 654 cm^{-1}) could imply an alteration of the perovskite symmetry because of the interaction with GDC.[56] In conclusion, the Raman spectrum of BCZY-GDC is not the result of the mere sum of the spectra of the single components and it reveals the occurrence of a peculiar configuration of defects likely related to the interfacial properties of the composite.

(Figure 3) shows the results of Raman temperature programmed analysis carried out on BCZY, GDC and BCZY-GDC, either in reducing atmosphere (4.58% H_2 in N_2) and in air after an oxidation step at 600 °C. For all samples, the spectra show a decrease of the intensity of the bands with the increase of temperature. Generally, in Raman analyses, an increase in temperature leads to a broadening and a reduction of band intensity, because of the increase in disorder due to thermal movement. In addition, all bands move towards lower Raman shift, due to the decreasing energy necessary to excite vibrations along progressively looser bonds.[31,53]
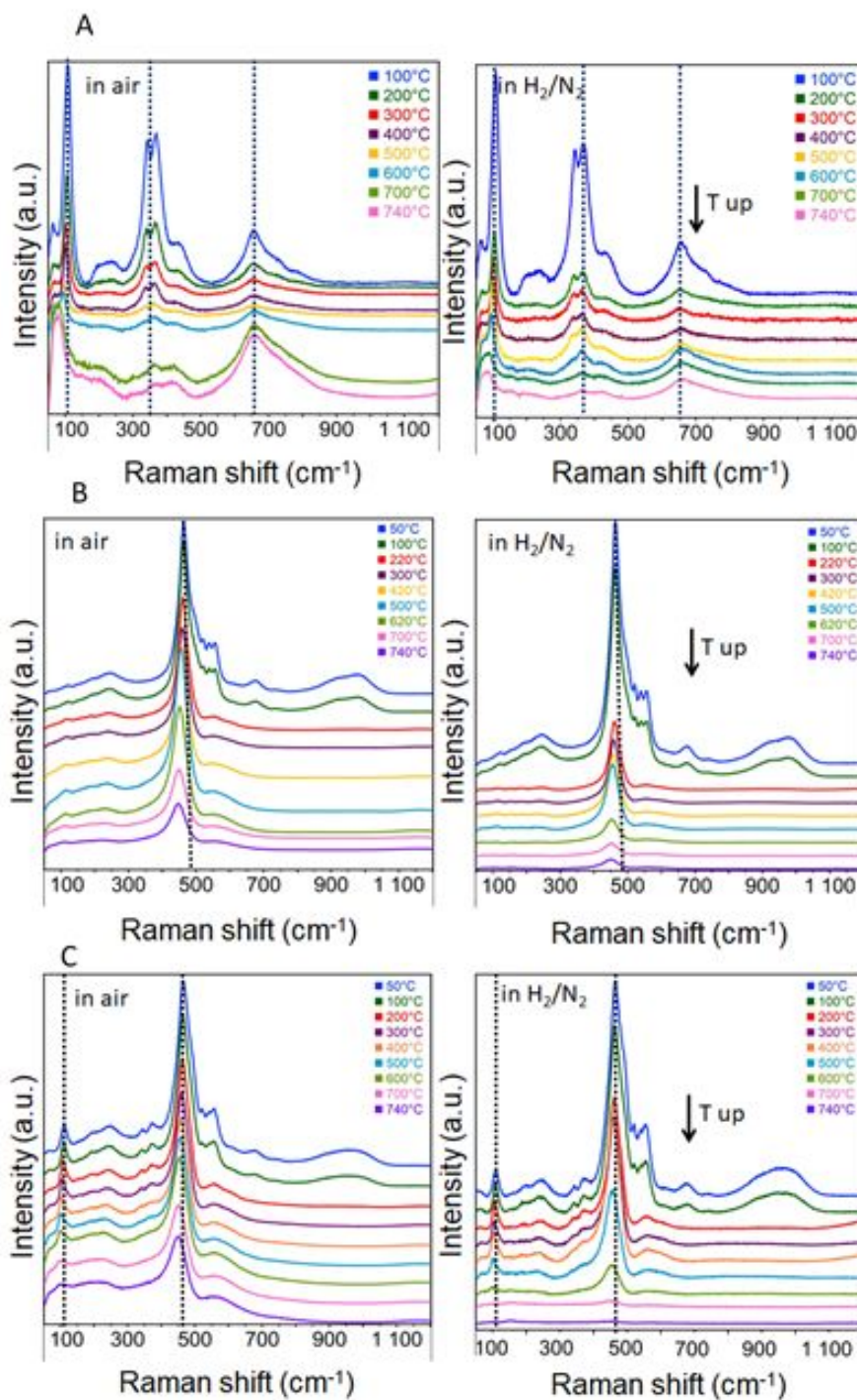
17

Figure 3: RAMAN spectra of single components during a heating ramp in different atmosphere of reaction: BCZY (A) and GDC (B), BCZY-GDC (C)

Another commonality between all samples is that the spectra acquired under reduced conditions show bands of lower intensity than spectra collected in air. which is probably due to the different absorption properties of the sample in the two atmospheres.[57] Under reducing atmosphere the thermal quenching of bands was also faster, especially for GDC and for the composite. Reduced samples resulted darkish and therefore the majority of excitation laser and scattering light is expected to be absorbed by the sample, rather than contribute to the Raman signal. Moreover, with the increase of oxygen vacancies within the material the concentration of metal cations increases compared to that of oxygen ions. This leads to a decrease in polarization and an increase in surface reflectivity which contribute to decrease the intensity of the Raman bands.[58] The effect of the thermal radiation of the oxides caused the signal to become very low and noisy especially above 680°C, thus making almost impossible to obtain information regarding the evolution of defects and changes of phases above 600°C. Bearing in mind all the above limitations the comparison among samples were carried out by the sequences of normalized spectra (see **(Figure S10, S11 and S12)** for BCZY, GDC and BCZY-GDC respectively).

In order to understand the changes observed for BCZY-GDC composite, we first investigated the thermal behavior of single components. For both BCZY and GDC the main spectra modifications were observed in the first stage of heating ramp and above 400°C. **(Table 3)** and **(Table 4)** summarize the results for BCZY and GDC, respectively.

19

Table 3: Trend of main relative changes of BCZY bands during thermal treatments

Temp. [°C]	BCZY bands* [cm⁻¹]			
	~108	~340-370	~420-430	~650
50-260	negligible changes	slight decrease of intensity	negligible changes	negligible changes
260-400	negligible changes	negligible changes	negligible changes	negligible changes
400-600	shift to lower wavenumbers	changes in the relative intensity, convergence to single peak at 360 cm^{-1}	negligible changes	increase intensity
600-740	fading and disappearance	decrease intensity	negligible changes	high intensity, slight shift to higher wavenumbers

* similar behaviour in air and in H_2

The results in Table 3 are consistent with previous studies that reported a change of the spectra in the range of 650-800°C, in correspondence of a phase transition from rhombohedral to cubic of the BCZY structure.[27,28] It is worth pointing out that in our case the transition was gradual and started already at around 500°C.

Table 4: Trend of main relative changes of GDC bands during thermal treatments

Temp. [°C]	GDC bands† [cm⁻¹]				
	~200	~463	~540-590	~680	~900-1000
50-260	negligible changes	very little broadening	higher in H_2, rapid decrease	fading to vanish	fading to vanish
260-500	slight increase	slight broadening	slight increase	disappeared	disappeared
500-740	increase of background above 680 °C appearance of peak at 150 cm^{-1} in H_2	broadening	increasing, more in H_2	disappeared	disappeared

†faster decrease in H_2; heat-related behaviour depending on the type of bands

From Table 4, it is clear that the thermal evolution of GDC spectrum is strongly correlated to the reorganization of surface defects and the formation of oxygen vacancies. The bands linked to vibrational modes involving oxygen vacancies decreased with different rates compared to the main peak at around 460 cm^{-1}. This limited the possibility of a quantitative analysis of the reduction process.[52] However, its qualitative analysis was estimated by normalizing the spectra collected above 600 °C and following the intensity ratio between the bands at ~570 cm^{-1} and ~ 463 cm^{-1}. The values of this parameter (I570/I460) were higher for the spectra collected in hydrogen than those measured in air **(Figure 4)**. Furthermore, in H_2 they reached a plateau because the reduction process origins an increase of intensity of the band at 570-600 cm^{-1} contrasting the opposite effect of temperature. On the other hand, during the air heating ramp the intensity of the bands decreases simultaneously but with different magnitude, which led to a linear increase in the I570/I460 ratio.

The evolution of the BCZY-GDC Raman spectrum during the heating treatments reflected the evolution of the spectra of the single components in air and in hydrogen flow (Figure 3C e Figure S12). However, some of the bands related to GDC overlapped with those of BCZY. For example, above 400°C, spectrum modifications in the range 500-650 cm^{-1} were attributed both to the phase transition of BCZY, and, under reduced conditions, also to the introduction of surface oxygen vacancies. This mainly involves the release of interstitial oxygen associated to MO_x defects in GDC[53] and the surface reduction of Ce^{4+} (see TPR paragraph). Taking this in mind, we used the ratio I570/I463 for a qualitative estimation of the reduction process in the composite, as done for the GDC (Figure 4b).
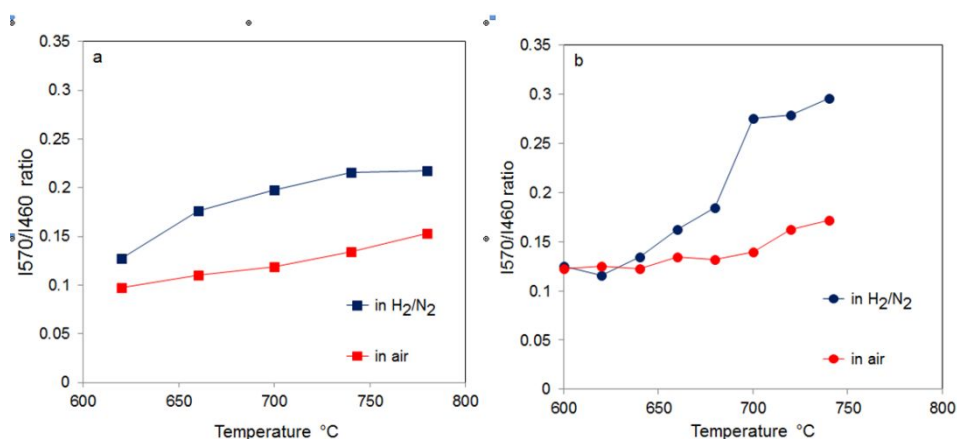
21

Figure 4: Evaluation of I570/I460 ratio under reducing and oxidizing heating ramp for (a) GDC and (b) BCZY-GDC

For all samples we followed the cooling ramps both in air and in H_2/N_2 (results not shown). The spectra collected in oxidizing conditions overlapped with those recorded during the heating ramp. This suggests that the structural changes were mainly related to the thermal expansion of the samples and were reversible. On the other hand, the thermal treatment in reducing condition led to a substantial modification of the final spectrum at room temperature in case of GDC and BCZY-GDC.

(Figure 5) showed the effect of a redox cycle on the materials investigated. In BCZY we registered some irreversible modifications in the intensity of bands and in their mutual ratio (see Figure 5a: bands at 340-370 cm^{-1} and ~670 cm^{-1} are higher in comparison to the peak at around ~108 cm^{-1}; moreover this latter band shifted to slight higher wavenumbers). This suggests that the redox thermal treatment affected the sub-lattice of A and B cations favoring a higher symmetry of the lattice. In GDC (Figure 5b) the intensity of peaks after reduction was very low due to the high absorbance of the reduced oxide, with the band at 560-600 cm^{-1} being almost a shoulder of the highest peak at 461cm^{-1}. It was possible to see the presence of a tiny peak at 150 cm^{-1}. No appropriate assignment could be found in literature for this peak;

22

however, the signal was clearly correlated with structural changes caused by the reduction.

After re-oxidation at 600°C the spectrum was similar to that of the initial oxidized sample, but

with a higher intensity of the bands at 520-560 cm^{-1}, at 676 cm^{-1} and of those centered at 943

cm^{-1}. All these bands were related to the presence of structural defects and oxygen

vacancies,[52,53,59] The fact that their intensity increased after a redox cycle suggests that the

oxide remained partially reduced.

In BCZY-GDC the thermal treatment under reducing condition led to a transformation of the

final spectrum at room temperature, with a strong attenuation of the peaks related to GDC in

comparison to those attributable to BCZY. The re-oxidation of the sample at 600°C allowed

recovering of the initial spectrum (Figure 5c).
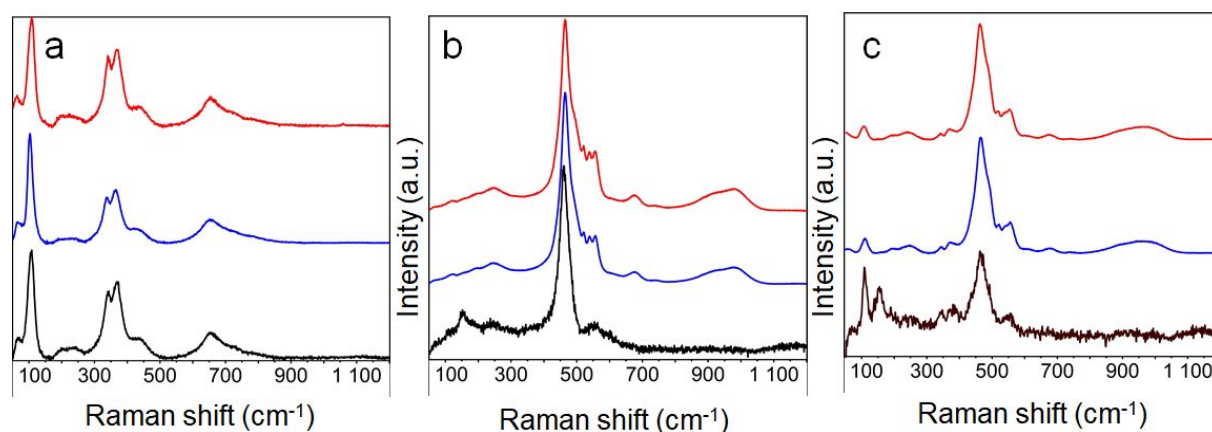
Figure 5: RAMAN spectra of oxidized (a) BCZY, (b) GDC and (c) BCZY-GDC before

(blue) and after (red) a redox cycle. Spectra in black are related to the samples after the ramp

in H_2/N_2

The medium-short distance structural changes detected in the bare BCZY and GDC after

the redox cycle were completely reversible in the composite, suggesting that BCZY and GDC

composite components synergistically counteracted their transformations mainly due to the

reduction process. We investigated the dynamics of this interaction by following the shift of

23

the main peak of the fluorite structure (peak at ~463 cm^{-1}) and of the orthorhombic structure (peak at ~108 cm^{-1}) of the BCZY-GDC. In fact, any difference from the general trend of this parameter, which is related to the thermal expansion of materials, should give information on the occurrence of interfering phenomena, such as reduction and structural changes, and about their impact on the involved structures.[55,59]

(Figure 6A) shows that the displacement of the peak at ~108 cm^{-1} followed the same trend both in hydrogen and in air, but it was less pronounced in BCZY-GDC composite than in pristine BCZY. Moreover, in the composite spectra we observed a phenomenon of anti-crossing at 500°C; i.e. the softening of the mode corresponding to the band at 108 cm^{-1} decreased abruptly. The accurate description of the anti-crossing phenomenon, which is usually attributed to the strong interaction between two different modes, would require further spectroscopic analyses and it is out of the scope of this study.[60] However, considering that at 500°C a symmetrisation of the perovskite was observed, we concluded that anti-crossing in the softening of band at 108 cm^{-1} could be taken as a descriptor of the R-3c→Pm-3m phase transition for the BCZY-GDC. This transition implies a contraction of the BCZY lattice; the different trend observed for the BCZY single phase material suggests that the thermal expansion of BCZY lattice in the composite is hindered by the presence of GDC and the effect is more relevant when the structure becomes cubic.

(Figure 6B) shows that the peak shift at ~ 461 cm^{-1} followed a similar trend for both GDC and BCZY-GDC, regardless of treatment atmosphere up to 600°C. At this temperature we observed anticrossing phenomena for both GDC and BCZY-GDC when the atmosphere of treatment is diluted H$_2$. Above 600°C there was a decrease in the extent of the shift with a greater effect on the GDC than on the composite. A deeper spectroscopic analysis would be required to describe in more detail this phenomenon; however we put forward an explanation based on the recent theoretical studies.[54,61] Muhich[61] proposed that the reduction of Ce^{4+} to the

24

larger Ce^{3+} cation is not the main cause of ceria lattice expansion. The elongation of Ce^{3+}--O^{2-} bond is counterbalanced by the concomitant contraction of neighboring Ce^{4+}-O^{2-} bonds and the long-distance expansion is rather due to an outward relaxation of Ce^{4+} neighboring the vacancy. This origins from the noncounterpoised attractive forces induced on Ce^{4+} cations by O anions 180 degrees opposite to the vacancy. This model agrees with recent calculations that demonstrated that a blue shift of F_{2g} Raman mode in CeO_{2-x} is expected if the lattice constant is not allowed to relax after defect creation.[54] Considering that the shift of the peak at 461 cm^{-1} accounts of the contribution due to the reduction of cerium,[55] the anti-crossing behavior observed in reducing condition should be correlated with the process of reduction. Under the experimental conditions, the formation of oxygen vacancies should have a compensatory effect on the softening of the mode caused by the thermal expansion. In this view, we attributed the differences in the trend between the two materials to a different number of vacancies.

From these results, it was possible to identify a critical temperature range (550°C-750°C) where the interaction between GDC and BCZY made GDC to thermally stabilize against the reaction atmosphere. Above 550°C the BCZY phase is cubic, and this structure can interact strongly with the cubic lattice of GDC, giving rise to more resistant and flexible interfacial bonds to comply with the effect of redox processes. These findings are consistent with the results of our recent study through *in-situ* synchrotron XRD characterization which demonstrated that, at high temperature, in humidified H_2, there is a synergistic effect between GDC and BCZY in the composite. This induces a thermal expansion of the individual components in favor of a greater reciprocal compatibility to thermo mechanical stress. [38]
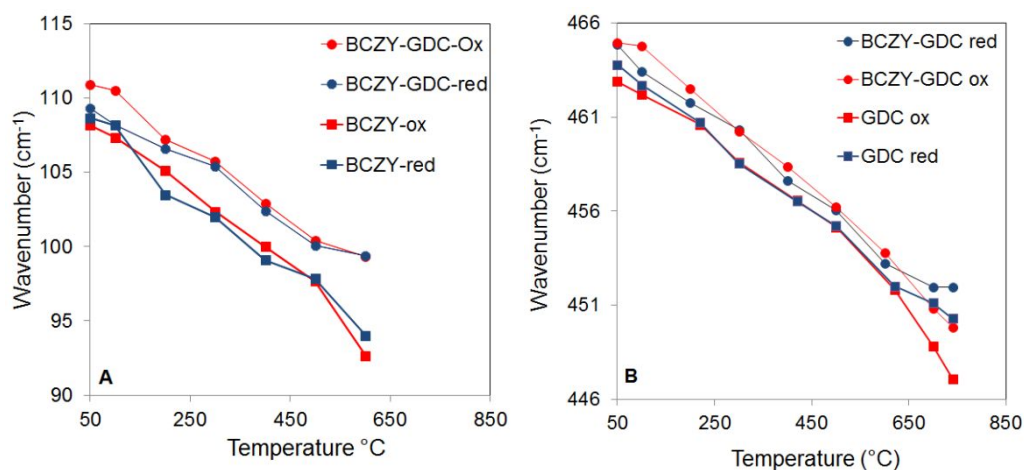
Figure 6: Trends of the shift for the peak at 108 cm^{-1} (A) and peak at ~464 cm^{-1} (B) in the single oxides and in the composite.

The redox flexibility and thermo-mechanical properties of this material would allow contrasting the strains induced by the expansion of ceria lattice in reducing conditions, especially when applied as structured component in devices such as fuel cells and membranes.

Temperature programmed analyses

XRD and Raman characterizations suggested that the high thermal stability and the reversibility of BCZY-GDC redox behavior was linked to a GDC lower propensity of being reduced in presence of BCZY. In order to verify this hypothesis and estimate the reducibility of the materials we carried out thermogravimetric analyses (TGA) and temperature programmed reduction measurements (TPR) on the samples under 4.58%H$_2$ in N$_2$ atmosphere.

(Figure 7) shows the results of TPR measurements. GDC and BCZY-GDC profiles show a small peak around 450°C related to the reduction of surface sites and a large signal at 750-800°C, attributable to the bulk reduction of Ce^{4+} to Ce^{3+} into the GDC lattice.
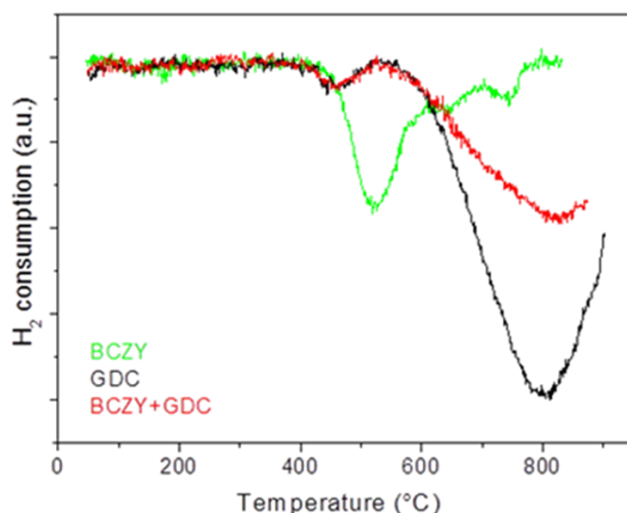
26

Figure 7: TPR profiles of BCZY, BCZY-GDC, GDC

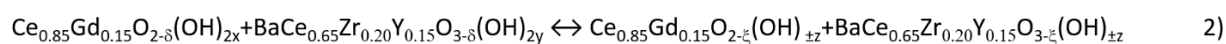TPR profile of BCZY shows a peak at about 500°C and two other small peaks at higher temperature, which are attributable to reduction of Ce^{4+} to Ce^{3+} in the BCZY lattice. TPR profiles are congruent with TGA results **(Figure S13)**. The quantitative results of TPR and TG analyses are reported in **(Table 3).** Because of the different configuration of the two experiments the consumption of H_2 measured during TPR experiments is not directly comparable with the amount estimable from the TGA profiles. However, qualitatively the results of the two analyses showed the same behavior, i.e. the degree of reduction of the composite was lower than what expected (16% vs 53%) from the reduction degree of the single components. The stability of the composite towards a redox treatment and the reproducibility of results have been proved performing two successive TPR after an isothermal oxidation step at 900°C **(Figure S14)**.

27

Table 3: Summary of TGA and TPR results

Samples	O_2 released from TGA	H_2 consumed in TPR
	[μmoles/g]	[μmoles/g][a]
GDC	326	1624
BCZY	157	193
BCZY-GDC	159	622

a-corresponding to a reduction of Ce^{4+} to Ce^{3+} of 66%, 18%, 16% from top to bottom

Therefore, it is established that the reduction of GDC in the BCZY-GDC composite is inhibited due to the interaction between the two components. The mechanism of interaction is summarized in (**Figure 8)** and the equilibrium at interface can be described by the reactions of (**Scheme 1**). At high temperature the incorporation of hydrogen as OH groups into the cubic lattice of BCZY and the simultaneous reduction of Ce^{4+} to Ce^{3+} with formation of water may lead in the interfacial zone to a local composition of adsorbed gases which shifts the equilibrium of reduction to the left.

$$Ce_{0.85}Gd_{0.15}O_{2-\delta} + BaCe_{0.65}Zr_{0.20}Y_{0.15}O_{3-\delta} + (x+y)\ H_2 \leftrightarrow Ce_{0.85}Gd_{0.15}O_{2-\delta}(OH)_{2x} + BaCe_{0.65}Zr_{0.20}Y_{0.15}O_{3-\delta}(OH)_{2y} \qquad 1)$$

$$Ce_{0.85}Gd_{0.15}O_{2-\delta}(OH)_{2x} + BaCe_{0.65}Zr_{0.20}Y_{0.15}O_{3-\delta}(OH)_{2y} \leftrightarrow Ce_{0.85}Gd_{0.15}O_{2-\xi}(OH)_{\pm z} + BaCe_{0.65}Zr_{0.20}Y_{0.15}O_{3-\xi}(OH)_{\pm z} \qquad 2)$$

Scheme 1: reactions describing the redox process occurring at BCZY-GDC interface, where OH groups can be H_2 or H_2O adsorbed, and $\zeta < \delta$.

This mechanism is supported by the fact that ceria reduction by H_2 involves the formation of hydroxyl groups as intermediates. Moreover, the reactivity of these latter depends on the configuration of vacancies and on the presence of strain in the oxide.[62,63]
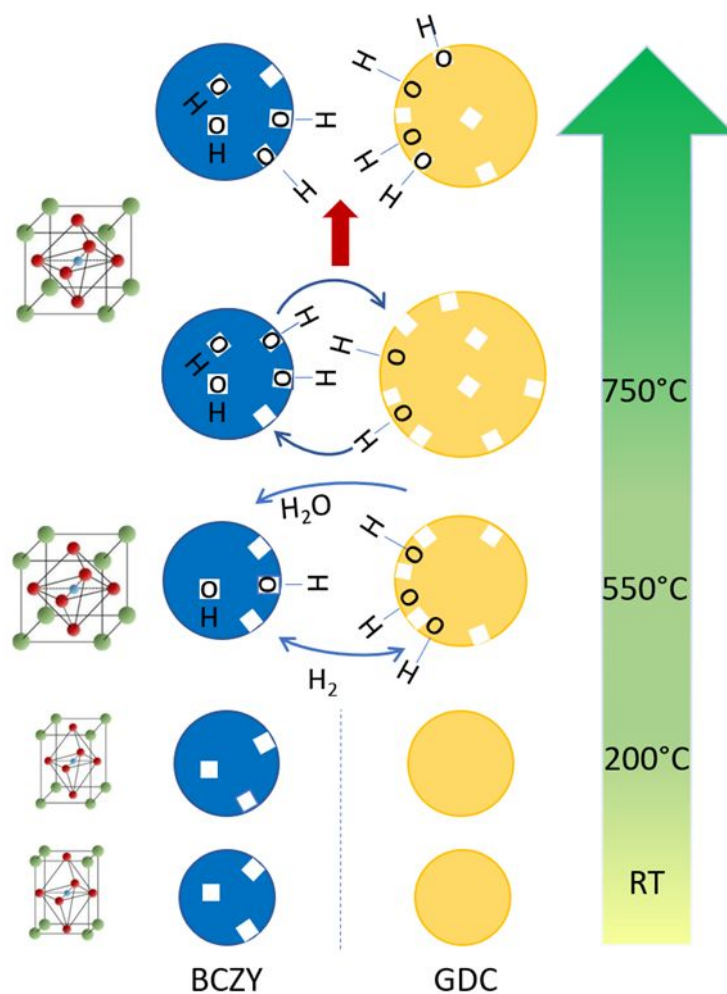
28

Figure 8: Representation of transformation and interaction of GDC and BCZY in the composite

CONCLUSION

This is the first study that focuses specifically on the redox behavior of the BaCe$_{0.65}$Zr$_{0.20}$Y$_{0.15}$O$_{3-\delta}$-Ce$_{0.85}$Gd$_{0.15}$O$_{2-\delta}$ (BCZY-GDC) dual-phase ceramic and its thermal and mechanical stability. BCZY-GDC showed full redox reversibility in comparison to the single oxides; its reduction involved mainly GDC, which was less reducible in the presence of

29

BCZY, thus allowing a higher thermal and mechanical robustness of the composite. Different techniques of analysis (TPR; TGA; *in-situ* RAMAN and *in-situ* XRD) under temperature programmed conditions revealed that the interaction between the single components occurred at nanoscale, impacting the redox behavior and the thermal resistance of BCZY-GDC especially at high temperature. At high temperatures and under reducing atmosphere, structural changes in the BCZY and the introduction of oxygen vacancies in the GDC lattice by Ce^{4+} reduction act synergistically determining interfacial processes able to limit the mechanical strains induced by the expansion of lattices with temperature and reduction.

This work highlights the importance of fundamental studies on redox behavior of perovskite-fluorite composites since they can reveal the occurrence of specific synergies between their components during operating conditions. This unexpected behavior would help engineering materials with enhanced functionalities in high temperature redox applications.

Supporting Information are available from the ACS Publications, free of charges. The PDF file contain supplementary data: Figure S1-S14, Table S1-S2.

Corresponding Author

*e-mail: marta.boaro@uniud.it

Author Contributions

The manuscript was written through contributions of all authors. All authors have given approval to the final version of the manuscript.

ACKNOWLEDGEMENTS

REFERENCES

[1] Z. Abdin, A. Zafaranloo, A. Rafiee, W. Mérida, W. Lipinski, K.R. Khalilpour, Hydrogen as an energy vector. *Renew. Sust. Energ. Rev*. **2020**, 120 109620.

[2] International Energy Agency, The future of Hydrogen, https://www.iea.org/reports/the-future-of-hydrogen, 2019.

[3] Hydrogen Council, How hydrogen empowers the energy transition, https://www.hydrogencouncil.com, report (2017).

[4] M. Marrony, *Protons ceramic conductors*, Taylor & Francis Group, LLC, Pan Stanford publishing, USA **2016.**

[5] H. Iwahara, Y. Asakura, K. Katahira, M. Tanaka, Prospect of hydrogen technology using proton-conducting ceramics. *Solid State Ionics* **2004**, 168, 299-310.

[6] J. Kim, S. Sengodan, K.O. Kwon, Y. Bud, G. Kim, Proton conducting oxides: A review of materials and applications for renewable energy conversion and storage, *Renew. Sust. Energ. Rev*. **2019**, 109, 606-618.

31

[7]   S. Hossain, A.M. Abdalla, S.N.B. Jamain, J.H. Zaini, A.K. Azad, A review on proton conducting electrolyte for clean energy and intermediate temperature-solid oxide fuel cell, *Renew. Sust. Energ. Rev.* **2017**, 79 750-764.

[8]   C. Duan, J. Tong, M. Shang, S. Nikodemski, M. Sanders, S. Ricote, A. Almansoori, R.O'Hayre, Readily processed protonic ceramic fuel cells with high performance at low temperature, *Science* **2015**, 349 1321-1326.

[9]   C. Duan, R. Kee, H. Zhu, N. Sullivan, L. Zhu, L. BIan, D. Jennings, R. Hayre, Highly efficient reversible protonic ceramic electrochemical cells for power generation and fuel production, *Nature Energy* **2019**, 4, 230-240.

[10]   H. Wang, X. Wang, B. Meng, X. Tan, K.S. Loh, J. Sunarso, S. Liu, Perovskyte base mixed protonic –electronic conducting membranes for hydrogen separation, recent status and advances, *J. Ind. Eng. Chem.* **2018**, 60 297-306.

[11]   S.S. Hashim, M.R. Somalu, K.S. Loh, S. Liu, W. Zho, J. Sunarso, Perovskite based proton conducting membranes for hydrogen separation: a review*, Int. J. Hydrogen Energy* **2018**, 43 15281-15305.

[12]   D. Medvedev, A. Brouzgou, A. Denim, P. Tsiakaras, in *Advances in Medium and High Temperatures Solid Oxide Fuel Cell Technology,* Vol. 574 (Eds. A. S. Aricò and, M. Boaro) Springer Nature, Cham, Switerland, **2017**, Ch.3.

[13]   K Singh, R. Kannan, V. Thangadurai, Perspective of perovskite-type oxides for proton conducting solid oxide fuel cells, *Solid State Ionics* **2019**, 339, 114951.

[14]   Z. Tao, Li Yan, J. Qiao, B. Wang, L. Zhang, A review of advanced proton-conducting materials for hydrogen separation, *Progr. Mat. Sci.* **2015**, 74, 1-50.

32

[15] N.R.L.M. Rashid, A.A. Samat, A.A. Jais, M.R Somalu, A. Muchtar, N.A. Baharuddin, W.N.R.W. Isahak, Review on zirconate-cerate-based electrolytes for proton-conducting solid oxide fuel cell, *Ceram. Inter.* **2019**, 45, 6605-6615.

[16] J. Huang, L. Zhang, C. Wang, P. Zhang, CYO–BZCYO composites with enhanced proton conductivity: Candidate electrolytes for low-temperature solid oxide fuel cells, *Int. J. Hydrogen Energy* **2012**, 37, 13044-13052.

[17] D. Medvedev, V. Maragou, E. Pikalova, A. Demin, P. Tsiakaras, Phase formation and properties of composite electrolyte $BaCe_{0.8}Y_{0.2}O_{3-\delta}$–$Ce_{0.8}Gd_{0.2}O_{1.9}$ for intermediate temperature solid oxide fuel cells, *J. Power Sources* **2013**, 221, 217-227.

[18] M.E. Ivanova, S. Escolástico, M. Balaguer, J. Palisaitis, Y. J, Sohn, W, A. Meulenberg, O. Guillon, J. Mayer & J. M. Serra, Hydrogen separation through tailored dual phase membranes with nominal composition $BaCe_{0.8}Eu_{0.2}O_{3-\delta}$:$Ce_{0.8}Y_{0.2}O_{2-\delta}$ at intermediate temperatures, *Nat. Sci. Rep.*, **2016**, 6, 34773 and reference therein.

[19] E. Rebollo, C. Mortalò, S. Escolastico, S. Boldrini, S. Barison, J. M. Serra, M. Fabrizio, Exceptional hydrogen permeation of all-ceramic composites robust membranes based on $BaCe_{0.65}Zr_{0.20}Y_{0.15}O_{3-\delta}$, *Energy Environ. Sci.* **2015**, 8, 3675-3688.

[20] D. Montaleone, Elisa Mercadelli, S. Escolastico, A. Gondolini, J. M. Serra, A. Sanson, All-ceramic Asymmetric membranes with superior hydrogen permeation, *J. Mater. Chem A*, **2018**, 6, 15718-15727.

[21] C. Mortalò, E. Rebollo, S. Escolastico, S. Deambrosis, K. Hass-Santo, M. Rancan, R. Dittmeyer, L. Armelao, M. Fabrizio, Enhanced sulfur tolerance of $BaCe_{0.65}Zr_{0.20}Y_{0.15}O_{3-d}$ -$Gd_{0.85}Gd_{0.15}O_2$ composite for hydrogen separation membrane*s, J. Membranes Sci*. **2018**, 564, 123-132.

33

[22] B. Zhu, L. Fan, P. Lund, Breakthrough fuel cell technology using ceria-based multi-functional nanocomposites, *Appl. Energy*, **2013**, 106, 163-175.

[23] L. Malavasi, C. Tealdi, C. Ritter, V. Pomjakushin, F. Gozzo, Y. Diaz-Fernandez, Combined neutron and synchrotrone X-Ray diffraction investigation of $BaCe_{0.85-x}Zr_xY_{0.15}O_{3-\delta}$ ($0.1 \leq x \leq 0.4$) protons conductors, *Chem. Mater.* **2011**, 23, 1323-1330.

[24] S. Tao, J.T.S. Irvine, Easily sintered proton-conducting oxide electrolyte for moderate-temperature fuel cells and electrolyzers, *Adv. Mater.* **2006**, 18, 1581-1584.

[25] S. Ricote, N. Bonanos, M.C. Marco de Luca, G. Caboche, Structural and conductivity study of proton conductor $BaCe_{0.9-x}Zr_xY_{0.1}O_{3-\delta}$ at intermediate temperatures, *J. Power Source* **2009** 193, 189-193.

[26] A. Slodczyk, M.D. Sharp, S. Upasen, P. Colomban, J.A. Kilner, Combined bulk and surface analysis of the $BaCe_{0.5}Zr_{0.3}Y_{0.16}Zn_{0.04}O_{3-\delta}$ (BCZYZ) ceramic proton-conducting electrolyte, *Solid State Ionics* **2014** 262, 870-874.

[27] C.-S. Tu, R.R. Chen, S.C. Lee, C.C. Huang, Temperature–dependent structure of proton conducting $Ba(Zr_{0.8-x}Ce_xY_{0.2})O_{2.9}$ ceramics by Raman scattering and x-ray diffraction, *J. Phys: Condens. Matter* **2012**, 24, 155403.

[28] F. Genet, S. Loridant, C. Ritter, G. Lucazeau, Phase transitions in $BaCeO_3$: neutron diffraction and Raman studies, *J. Phys. Chem. Solid.* **1999**, 60, 2009-2021.

[29] I. Charrier-Cougolic, T. Pagnier, G. Lucazeau, Raman Spectroscopy of perovkite-type $BaCe_xZr_{1-x}O_3$ ($0 \leq x \leq 1$), *J. Solid State Chem.* **1999**, 142, 220-227.

[30] C. Artini, M. Pani, A. Lausi, R. Masini, G. A. Costa, High temperature structural study of Gd-doped ceria by synchrone X-Ray diffraction (673 K≤T≤1073 K), *Inorg. Chem.* **2014**, 53 10140-10149.

[31] C. Artini, S. Presto, S. Massardo, M.Pani, M.M. Carnasciali, M. Viviani, Transport properties and high temperature Raman feature of heavily Gd-doped Ceria, Energies, *Energies*. **2019**, 12, 4148-1-11.

[32] K.D. Kreuer, Proton-Conducting Oxides, *Annu. Rev. Mater. Res.* **2003**, 33, 333-359.

[33] K.D. Kreuer, Aspects of the formation and mobility of protonic charge carriers and the stability of perovskite-type oxides, *Solid State Ionics* **1999**, 125, 285-302.

[34] R. Schmitt, A. Nenning, O. Kraynis, R. Korobko, A.I. Frenkel, I. Lubomirsky, S.M. Haile, J.L.M. Rupp, A review of defect structure and chemistry in ceria solid solutions, *Chem Soc. Rev,* **2020**. 49,554-592.

[35] A.Trovarelli,, Structural and Oxygen Storage/Release Properties of CeO_2-Based Solid Solutions *Comm. Inorg. Chem.,* **1999**, 20, 263-284.

[36] G. Hudish, A. Manerbino, W.G. Coors, S. Ricote, Espansions in $BaZr_{0.9-x}Ce_xY_{0.1}O_{3-\delta}$ (x= and 0.2) upon hydration determined by high-temperature X-ray diffraction, *J. Chem. Am. Ceram. Soc.* **2018**, 101, 1298-1309.

[37] A.K. Andersson, S.M. Selbach, C.S. Knee, T. Grande, Chemical expansion due to hydration of proton-conducting perovskite oxide ceramics, *J. Am. Ceram. Soc.* **2014**, 97, 2654-2661.

35

[38] C. Mortalò, A. Santoru, C. Pistidda, E. Rebollo, M. Boaro, C. Leonelli, M. Fabrizio, Structural evolution of $BaCe_{0.65}Zr_{0.20}Y_{0.15}O_{3-\delta}$-$Ce_{0.85}Gd_{0.15}O_{2-\delta}$ composite MPEC membrane by in-situ synchrotron XRD analyses, *Mat. Today Energy* **2019**, 13, 331-341.

[39] A.C. Larson; R.B. Von Dreele. General Structure Analysis System (GSAS), *Los Alamos National Laboratory Report LAUR 86-748* **2000**.

[40] B.H. Toby, EXPGUI, a graphical user interface for GSAS, *J Appl Crystallogr* **2001**, *34*, 210-213.

[41] A. Pappacena, P. Porreca, M. Boaro, C. de Leitenburg, A. Trovarelli, Effect of process modification and presence of H_2O_2 in the synthesis of samaria-doped ceria powders for fuel cell applications, *Int. J. Hydrogen Energy*. **2012**, 37, 1698-1709.

[42] R. Schmitt, A. Nenning, O. Kraynis, R. Korobko, A.I. Frenkel, I. Lubomirsky, S.M. Haile, J.L.M. Rupp, Study of oxygen vacancies in $Ce_{0.9}Pr_{0.1}O_{2-\delta}$ by X-ray diffraction and in situ Raman spectroscopy, *Chem Soc. Rev.* **2020**, 49, 554-592.

[43] I. Luisetto, S. Tuti, C. Romano, M. Boaro, E. di Bartolomeo, J. K. Kesavan, . S.S. Kumar, K. Dry reforming of methane over Ni supported on doped CeO_2: New insight on the role of dopants for CO_2 activation, *J. CO$_2$ Utilization*, **2019,** 30, 63-78.

[44] A. Slodczyk, O. Zaafrani, M.D. Sharp, J.A. Kilner, B. Dabrowski, O. Lacroix and P. Colomban, Testing the chemical/structural stability of proton conducting perovskite ceramic membranes by in situ/ex situ autoclave raman microscopy, *Membranes* **2013,** 3, 311-330.

[45] F. Genet, S. Loridant and G. Lucazeau, Vibrational normal modes of the D_{2h}^{16} phase of $BaCeO_3$ a critical comparison of force fields, *J. Raman Spect.* **1997**, 28, 255-276.

36

1
2
3
4
5
6
7
8
9
10
11
12
13
14
15
16
17
18
19
20
21
22
23
24
25
26
27
28
29
30
31
32
33
34
35
36
37
38
39
40
41
42
43
44
45
46
47
48
49
50
51
52
53
54
55
56
57
58
59
60

[46] T. Scherban, R. Villeneuve, L. Abello, G. Lucazeau Raman scattering study of acceptor-doped $BaCeO_3$, *Solid State Ionics* **1993**, 61, 93-98.

[47] M. Arrigoni, E. A. Kotomin, J. Maier. Large-scale modeling of defects in advanced oxides: Oxygen vacancies in $BaZrO_3$ crystals, in *High performance Computing Science and Engineering* Vol. 15 (eds.W.E. Nagel, D.H. Kröner, M.M. Resch) Springer, Cham, Switerland, **2016**, pp. 187-198.

[48] D. Han, M. Majima, T. Uda, Structure Analysis of $BaCe_{0.8}Y_{0.2}O_{3-\delta}$ in Dry and Wet Atmospheres by High-Temperature X-ray Diffraction Measurement, *J. Solid State Chem.* **2013** 205, 122-128.

[49] A. Banerji, V. Grover, V. Sathe, S.K. Deb, A.K. Tyagi, CeO_2 Gd_2O_3 system: Unraveling of microscopic features by Raman spectroscopy, *Solid State Comm.* **2009**, 149, 1689-1692.

[50] W.Y. Hernández, O.H. Laguna, M.A. Centeno, J.A. Odriozola, Structural and catalytic properties of lanthanide (La, Eu, Gd) doped ceria, *J. Solid State Chem.* **2011**, 184, 3014-3020.

[51] Y. Xu, F. Wang, X. Liu, Ya Liu, M. Luo, B. Teng, M. Fan, X. Liu, Resolving a decade-long question of oxygen defects in Raman spectra of ceria-based catalysts at atomic level, *J. Phys. Chem. C* **2019**, 123, 18889-18894.

[52] E. Sartoretti, C. Novara, F. Giorgis, M. Piumetti, S. Bensaid N. Russo, D. Fino, In situ Raman analyses of the soot oxidation reaction over nanostructured ceria based catalyst, *Nat. Sci. Rep*. **2019**, 9, 3857 and reference therein.

[53] C. Andriopoulou, A. Trimpalis, K. C. Petallidou, A. Sgoura, A. M. Efstathiou, S. Boghosian. Structural and redox properties of $Ce_{1-x}Zr_xO_{2-\delta}$ and $Ce_{0.8}Zr_{0.15}Re_{0.05}O_{2-\delta}$ (RE:La,

Nd, Pr, Y) solids studies by high temperature in situ Raman spectroscopy, *J. Phys. Chem.* C **2017**, 121, 7931-7943.

[54]   V.V.C. Schilling, A. Hofmann, C. Hess, M.V. Ganduglia-Pirovano, Raman spectra of polycrystalline CeO_2: A density functional theory study, *J. Phys. Chem.* C **2017**,121, 20834-20849.

[55]   J.R. McBride, K.C. Hass, B.D. Poindexter, W.H. Weber, Raman and X-ray studies of $Ce_{1-x}Re_xO_{2-y}$ where Re= La, Pr, Nd, Eu, Gd, and Tb, *J. Appl. Phys.* **1994**, 76, 2435-2441.

[56]   P. Colomban, A. Slodczyk, Raman intensity: An important tool to study the structure and phase transitions of amorphous/crystalline materials, *Opt. Mater.* **2009**, 31, 1759-1763.

[57]   M. Guo, J. Lu, Q. Bi, M. Luo, Effect of optical absorbance on Raman spectra of $Ce_{0.9}Tb_{0.1}O_{2-\delta}$ solid solution, *Chem. Phys. Chem.* **2010**, 11, 1693-1699.

[58]   R.C. Maher, L.F. Cohen. Raman Spectroscopy as a probe of temperature and oxidation state for gadolinum-doped ceria used in solid oxide fuel cells, *J. Phys Chem A.* **2008**, 112 1497-1497.

[59]   L- Li, F. Chen, J-Q. Lu, M.-F. Luo, Study of defect site in $Ce_{1-x}M_xO_{2-\delta}$ (x=0.2) solid solution using Raman spectroscopy, *J. Phys. Chem. A* **2011**, 115, 7972-7977.

[60]   G. Lucazeau, Effect of pressure and temperature on Raman spectra of solids: anharmonicity, *J. Raman Spect.* **2003**, 34, 478-496.

[61]   C. L. Muhich, Re-evaluating CeO_2 Expansion Upon reduction: non counterpoised forces, not ionic radius effects, are cause *J. Phys. Chem C.* **2017**, 121, 8052-8059.

[62]   M. García-Melchior, Núria López, Homolytic Products from Heterolytic paths in H_2 dissociation on metal oxides: The example of CeO_2, *J. Phys. Chem*, **2014**, 118, 10921-10926.

38

[63] Y. Gao, R. Li, S. Chen, L.Luo, T. Lao, W. Huang, Morphology-dependent interplay of reduction behaviors, oxygen vacancies and hydroxil reactivity of CeO_2 nanocrystal, *Phys. Chem. Chem. Phys.* **2015**, 17, 31862-31871.

Table of contents:

The redox behavior of $BaCe_{0.65}Zr_{0.20}Y_{0.15}O_{3-\delta}$-$Ce_{0.85}Gd_{0.15}O_{2-\delta}$ is investigated with a multi analytical approach to understand the impact of different operating conditions on its stability. Structural changes and redox reactions are observed depending on the operating conditions. Conversely to what expected, these processes play synergistically to stabilize the composite at high temperature thank to an interfacial equilibrium that involves oxygen vacancies defects and protons.